COMPUTER-AIDED CIVIL AND INFRASTRUCTURE ENGINEERING

Computer-Aided Civil and Infrastructure Engineering **31** (2016) 366–380

Optimal Mainline Variable Speed Limit Control to Improve Safety on Large-Scale Freeway Segments

Zhibin Li, Pan Liu, Chengcheng Xu & Wei Wang*

Jiangsu Key Laboratory of Urban ITS, Southeast University, Nanjing, China and Jiangsu Province Collaborative Innovation Center of Modern Urban Traffic Technologies, Nanjing, China

Abstract: *The primary objective of this study was to develop a procedure for determining the optimal variable speed limit (VSL) control strategy that aims at reducing both collision risks and injury severity on large-scale freeway segments. The achieved reduction in collision risks and injury severity were evaluated using real-time crash risk and severity prediction models. A modified cell transmission model (CTM) that took into consideration the capacity drop and the stop-and-go traffic was used to simulate the traffic operations with the VSL control. A computational procedure that incorporated the genetic algorithm and the CTM was proposed for the optimization of critical VSL control factors. Three scenarios with various placements of VSL signs on freeway mainlines were evaluated. The results showed that the optimal VSL control successfully decreased the collision risks by 22.62% and reduced the injury severity of crashes by 14.67%. We also evaluated how drivers' compliance to speed limits affected the effectiveness of VSL control. The safety effects decreased as drivers' compliance rate to the VSL control decreased. The finding suggests the use of speed enforcement techniques together with the VSL control to achieve the optimum control effects.*

1 INTRODUCTION

Variable speed limit (VSL) is a traffic control technique that has been increasingly used to reduce crash risks on freeway mainlines. The central idea of VSL control is to make an intervention proactively by adjusting speed limits posted on roadside VSL signs. Previous studies have proposed numerous VSL control strategies that focus on reducing collision risks on freeways (Robinson, 2000; Hooshdar and Adeli, 2004; Adeli and Karim, 2005; Lee et al., 2006; Abdel-Aty et al., 2006; Allaby et al., 2007; Adeli and Jiang, 2009; Hellinga and Mandelzys, 2011; Tazul Islam et al., 2013; Lee et al., 2013; Hadiuzzaman and Qiu, 2013; Li et al., 2014a, b). The control factors considered previously include the start-up threshold, the rate at which the speed limit is changed, and the coordination between consecutive VSL signs.

Most of the previous studies have only considered the VSL control strategies for relatively short freeway segments (1 to 6 miles) with homogeneous traffic flow characteristics (Lee et al., 2006; Allaby et al., 2007; Li et al., 2014a, b). VSL control strategies developed for different freeway sections could be difficult to be coordinated given distinct control logic. Uncoordinated VSL control may bring disturbances to freeway traffic, resulting in increased collision potentials. In addition, the following critical issues have not been addressed in previous studies: (1) the optimum placement of VSL signs; (2) the transferability of VSL control strategy; (3) the effects of drivers' compliance rate to posted speed limits on the effectiveness of VSL control; and (4) the effects of VSL control on the severity of crashes. These issues may negatively affect the use of proposed VSL control strategies in practical engineering applications.

The primary objective of this study was to develop a procedure for determining the optimal VSL control strategy that aims at reducing both collision risks and injury severity on large-scale freeway segments. A computational procedure that incorporated the genetic algorithm (GA) was used to optimize VSL control strategies. The crash risk and severity prediction models that were developed in the authors' previous study were used to predict the collision risks and the severity of crashes given simulated traffic parameters. Various scenarios with different placements of VSL signs were evaluated. We also evaluated how the drivers' compliance to the posted speed limit affected the effectiveness

*To whom correspondence should be addressed. E-mail: *wangwei@seu.edu.cn*.

DOI: 10.1111/mice.12164

of the proposed VSL control strategy. Finally, the effects of the proposed VSL control strategy were validated using another freeway section.

2 CRASH PREDICTION MODELS

Before evaluating the safety effects of VSL control, relationships must be established between traffic collisions and freeway traffic flow parameters. Previously, numerous crash risk prediction models have been developed to evaluate the collision risks given real-time loop detector data (Lee et al., 2003; Oh et al., 2005; Abdel-Aty et al., 2005; Xu et al., 2012a; Li et al., 2013). However, previous models have not focused on the injury severity associated with a crash that occurred on freeways. In this study, the crash risk and severity prediction models that were developed in the authors' previous study were used to predict the collision risks as well as the crash injury severity (Xu et al., 2013). The model development was briefly discussed here.

Crash data and traffic flow data were collected from the 29-mile freeway sections on the Interstate-880 in the state of California. Traffic flow data prior to the occurrence of crashes and traffic flow data that did not result in any crashes were selected. Previously, various types of crash prediction models have been developed (see a summary in Xu et al., 2012). Among them, the binary logit model was the most commonly used method to fit the crash data in which the response variable is binary, that is, crash versus non-crash (Abdel-Aty et al., 2005; Xu et al., 2012; Zheng et al., 2010; Oh et al., 2005). As compared to other non-parametric or artificial intelligent models, the binary logit model provides clear and straightforward relationships between collision risks and traffic flow parameters.

The sequential logit models were developed to predict the collision risks and the injury severity. The study considered two levels of injury severity: fatal/injury (FI), and property-damage-only (PDO). The modeling structure included two stages: (1) stage 1: crash cases (binary response = 1) versus non-crash cases (binary response = 0); and (2) stage 2: FI injuries (binary response = 1) versus PDO injuries (binary response = 0). The binary logit model was applied at each stage to fit the developed sequential logit model. With the binary logit model, the probability of an event occurrence can be estimated using the following equation:

$$P(Y=1)=\frac{1}{1+e^{-g(x_i)}} \tag{1}$$

where $P(Y=1)$ denotes the probability of crash occurrence or FI injury severity, and $g(x_i)$ is the utility function that is linear combination of explanatory variables which can be expressed as:

$$g(x)=\beta_0+\beta_1 x_1+\ldots+\beta_k x_k \tag{2}$$

where x_k denotes the value of traffic variable k and β_k is the coefficient of variable k.

Initially, 33 explanatory variables were considered for the development of crash prediction models. Those variables represented the average and the standard deviation of traffic at the upstream and the downstream loop detector locations in each link, the differences of traffic between the upstream and the downstream links and between different lanes, and the road geometric designs. The parameters of variables in the model were estimated by the maximum likelihood estimation approach. The variables that were not significant at a 90% confidence level were excluded from model. The model form that had the largest R^2 and the smallest Akaike information criterion was considered the final one (Washington et al., 2010).

Finally, eight variables were found to be significantly related to the collision risks, including the 5-minute average occupancy at upstream station (x_{i1}), the 5-minute standard deviation of speed at upstream station (x_{i2}) and downstream station (x_{i3}), the 5-minute average absolute difference in occupancies between adjacent lanes at upstream station (x_{i4}), the 5-minute absolute difference in vehicle counts between upstream and downstream stations (x_{i5}), the 5-minute absolute difference in occupancies between upstream and downstream stations (x_{i6}), the spacing between upstream and downstream station (x_{i7}), the road surface width (x_{i8}), outer shoulder width ($x_{i9}=1$, if width >10 ft; $x_{i9}=0$, otherwise), and curve ($x_{i10}=1$, if curve section; $x_{i10}=0$, otherwise). The utility function in the collision risk prediction model can be estimated by:

$$\begin{aligned} g_i(x) = {} & -2.672+0.074x_{i1}+0.060x_{i2}+0.050x_{i3} \\ & +0.119x_{i4}+0.092x_{i5}+0.026x_{i6}+1.057x_{i7} \\ & -0.049x_{i8}-0.856x_{i9}+0.508x_{i10} \end{aligned} \tag{3}$$

The 5-minute average occupancy at upstream station (x_{j1}), the 5-minute average vehicle count at downstream station (x_{j2}), the peak period ($x_{j3}=1$, if peak period; $x_{j3}=0$, otherwise), and the road surface width (x_{j4}) were found to be significantly related to the FI injury once a crash occurred. The utility function in the injury severity prediction model can be estimated by:

$$\begin{aligned} g_j(x) = {} & 2.129-0.033x_{j1}-0.056x_{j2}-0.335x_{j3} \\ & -0.036x_{j4} \end{aligned} \tag{4}$$

Given the utility functions, the probability of collision, denoted by $P(\text{crash} = 1)$ and the probability of FI injury severity, denoted by $P(\text{FI} = 1)$ can be estimated by the binary logit model.

3 DEVELOPMENT OF SIMULATION MODEL

Several previous studies have used microscopic simulation models to evaluate the safety effects of VSL (Lee et al., 2006; Abdel-Aty et al., 2006; Allaby et al., 2007; Hellinga and Mandelzys, 2011). Even though microscopic models have the advantage in capturing the individual vehicle movements, they may not be the optimum solution to capture the macroscopic characteristics of some unique traffic flow phenomenon observed on freeways. Some studies suggested that capacity drop was caused by a "void" made by slow lane changes (Laval and Daganzo, 2006; Leclercq et al., 2011), but other researchers concluded that capacity drop was caused by the impact of stop-and-go waves (Oh and Yeo, 2012). As the occurrence mechanism of capacity drop is not well understood, in microscopic models it is still not clear how the parameters in the car-following and the lane-changing models can be calibrated such that the simulation models provide reasonable estimates for different levels of capacity drop and stop-and-go waves.

This study used the cell transmission model (CTM) for the simulation of traffic flow on freeway mainlines where VSL control was used. The CTM is a mesoscopic simulation approach proposed based on the kinematic wave theory (Daganzo, 1994). The CTM can be easily calibrated using routinely available loop detector data and can be extended to large-scale freeways or networks (Li et al., 1999; Ukkusuri and Waller, 2008; Lin et al., 2011; Muñoz et al., 2006; Gomes et al., 2008). In this study, thousands of simulation runs need to be performed to determine the optimal VSL control factors. The CTM requires much less computational workloads and runs much faster as compared to microscopic simulation models.

Another reason for selecting the CTM lies in the fact that the decision of VSL control is usually made on the basis of aggregated traffic data from inductive loop detectors. For example, the resolution of traffic data reported from loop detectors is usually 30 seconds. Accordingly, the crash risk prediction models established relationships between crash risks and macroscopic traffic flow parameters which were usually estimated with the aggregated data in the 5-minute intervals. Until recently, it is still not so clear as to how VSL control affects the behavior of individual drivers, and how the behavior of individual drivers can be connected to macroscopic traffic flow parameters and collision risks. As a result, detailed information from individual vehicles is actually not considered in the VSL control strategy. The use of aggregated traffic data in the evaluation of collision risks further justifies the use of CTM in this study.

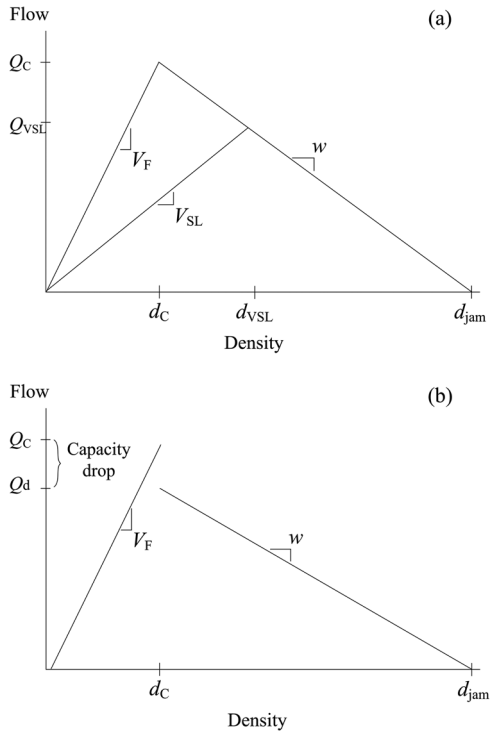

Fig. 1. (a) Fundamental diagram of traffic flow in CTM and (b) fundamental diagram with capacity drop.

3.1 Development of CTM with VSL control

By dividing freeway into sub sections, that is, cells, the CTM predicts the macroscopic traffic flow characteristics within each cell by evaluating the flow and density at a finite number of intermediate points. The length of the cell is chosen such that it is equal to the distance traveled by free-flow traffic in each evaluation time step. The traffic state is assumed to be homogeneous within each cell and is evaluated for each time step. Traffic in a cell operates according to the fundamental diagram that can be approximated by a triangular shape in the CTM.

As shown in Figure 1, the left slope of the triangular-shaped fundamental diagram represents the free-flow traffic states, whereas the right slope represents the congested traffic state. The slopes of the two sides and the apex of the triangle are the parameters in the CTM that need to be calibrated. To more accurately reproduce the

traffic flow affected by the VSL control, modifications need to be made to the fundamental diagram. Assuming that cell i is characterized by its triangular-shaped fundamental diagram, the left limb of the triangle in Figure 1a represents the sending function and the right limb represents the receiving function. The sending function represents the vehicles that supply to the downstream cell i+1 with a flow of $s_i(k)$, where k is the time step. The receiving function represents the available space in cell i which determines how many vehicles can enter cell i from the upstream cell i–1 with a flow of $r_i(k)$.

With the control of VSL, the sending and receiving functions are determined by the reduced speed limit rather than the free flow speed. The sending and the receiving functions for a cell i affected by the VSL control can then be determined by:

$$s_i(k) = \min\left\{V_{\mathrm{SL}}(k) \cdot d_i(k) \cdot n_i,\, Q_{\mathrm{VSL}}\right\}, \quad \text{where } V_{\mathrm{SL}}(k) \in [V_{\min}, V_{\mathrm{F}}] \tag{5}$$

$$r_i(k) = \min\left\{w_i \cdot \left(d_{i,\mathrm{jam}} - d_i(k)\right) \cdot n_i,\, Q_{\mathrm{VSL}}\right\} \tag{6}$$

where $s_i(k)$ is the sending flow (veh/h) at time k, $r_i(k)$ is the receiving flow (veh/h), V_{F} is the free flow speed (mph), $V_{\mathrm{SL}}(k)$ is the speed limit (mph) posted on the VSL sign at time k, $V_{\min}$ is the minimum allowed speed limit (mph), $d_i(k)$ is the density (veh/mile/ln), n_i is the number of lanes, Q_{VSL} is the maximum flow (veh/h) under current speed limit, w_i is the speed of the kinematic wave (mph), and $d_{i,\mathrm{jam}}$ is the jam density (veh/mile/ln).

The fundamental diagram determines three traffic flow parameters: the free-flow speed, the capacity flow per lane, and the speed of kinematic wave. Considering the fact that the three traffic parameters on the same freeway are roughly identical, we used a single fundamental diagram for the segment cells in the CTM. The flow in a cell i can be determined by the sending and the receiving functions:

$$q_i(k) = \min\left\{s_{i-1}(k), r_i(k)\right\} \tag{7}$$

The density evolution in cell i can be determined by the following equation:

$$d_i(k+1) = d_i(k) + \Delta T / (L_i \cdot n_i) \cdot (q_{i-1}(k) - q_i(k)) \tag{8}$$

where ΔT is the length of the simulation time step, which equals the time with which a vehicle passes a cell at free-flow speed, and L_i is the length (mile) of cell i.

The speed within each cell i can be determined according to the current density and speed limit:

$$v_i(k) = \begin{cases} \min\left\{V_{\mathrm{F}}, V_{\mathrm{SL}}(k-1)\right\} & \text{if } d_i(k) \le d_{\mathrm{VSL}} \\ (d_{i,\mathrm{jam}}(k) - d_i(k)) \cdot w_i / d_i(k) & \text{if } d_i(k) > d_{\mathrm{VSL}} \end{cases} \tag{9}$$

where d_{VSL} is the density (veh/mile/ln) associated with the flow Q_{VSL} under the speed limit V_{SL}.

The occupancy $o_i(k)$ in the CTM was calculated by the density $d_i(k)$ and the jam density $d_{i,\mathrm{jam}}$, which is:

$$o_i(k) = d_i(k) / d_{i,\mathrm{jam}}. \tag{10}$$

3.2 Generation of capacity drop and stop-and-go traffic

Capacity drop represents the fact that the discharge flow at an active bottleneck drops below the bottleneck capacity after congestion forms at the bottleneck area (Cassidy and Rudjanakanoknad, 2005; Chung et al., 2007; Oh and Yeo, 2012). To simulate the magnitude of capacity drop at the bottleneck, we assumed that the bottleneck cell i was characterized by an inverse λ-shaped fundamental diagram (see the dashed line in Figure 1b). The sending and the receiving functions for cell i with capacity drop being considered can be determined by:

$$s_i(k) = \begin{cases} V_{\mathrm{F}} \cdot d_i(k) \cdot n_i & \text{if } d_i(k) \le d_{\mathrm{C}} \\ Q_{\mathrm{d}} & \text{if } d_i(k) > d_{\mathrm{C}} \end{cases} \tag{11}$$

$$r_i(k) = \begin{cases} Q_{\mathrm{c}} & \text{if } d_i(k) \le d_{\mathrm{C}} \\ w_i \cdot (d_{i,\mathrm{jam}} - d_i(k)) \cdot n_i & \text{if } d_i(k) > d_{\mathrm{C}} \end{cases} \tag{12}$$

where Q_{c} is the capacity of the bottleneck (veh/h) and Q_{d} is the maximum discharge flow rate (veh/h) after capacity drop.

Traditional CTM is unable to generate the stop-and-go traffic. Traffic congestion in the traditional CTM simulation is much more smoothed than in the reality. Safety issues happen not only at the tail of the congestion but also within the congestion. The CTM should provide accurate estimates for the stop-and-go traffic. In previous studies, researchers have made modifications in the CTM to reflect the stochastic feature in the traffic flow (Sumalee et al., 2011; Li et al., 2009; Kim and Zhang, 2008; Boel and Mihaylova, 2006).

In this study, we introduced a stochastic component into the CTM to generate the stop-and-go traffic in congestion. According to Figure 1a, the traffic flow within a cell was determined by the receiving function if the traffic is congested. In the stochastic CTM, the receiving function for the bottleneck cell was determined by

$$s(k) = s(k) + e(k) \tag{13}$$

$$e(k) = \varphi \cdot s(k) \cdot \varepsilon(k)], \text{where } \varepsilon(k) \in [-1, 1] \tag{14}$$

where e(k) is the stochastic component at time k, $\varepsilon(k)$ is the generated random noise at time k, and φ is the parameter which determines the magnitude of the stop-and-go wave. A stop-and-go wave was generated

according to the probability threshold, which is given by:

$$s(k) = s(k) + e(k), \text{if } \zeta(k) < \phi \text{ and } v(k) < V_{TH} \quad (15)$$

$$s(k) = s(k), \text{else} \quad (16)$$

where $\zeta(k)$ is random number within [0, 1], ϕ is the probability threshold, and V_{TH} is the speed threshold to determine if the traffic is congested. After the stop-and-go waves are generated, those waves propagate toward upstream sections at relatively constant speeds. The calibration of the parameter φ and ϕ was presented in later sections.

3.3 Calculation of aggregated loop detector data in CTM

In this study the length of each cell was set to be 0.1 mile. The free-flow speed was 65 mph in the selected freeway. Thus, the time step in the simulation in the CTM was 5.54 seconds. In the crash prediction model developed in Section 2, the traffic variables that were used to predict crash risks and injury severity were calculated based on aggregated traffic data. The traffic variables in the 5-minute interval were calculated by the reported loop detector data with a resolution of 30 seconds. In the CTM-based simulation, traffic data were aggregated to support the estimation in the crash prediction models.

The cells where loop detectors were located were identified in the CTM. Traffic parameters in those cells were used as spot parameters in loop detectors, assuming traffic was homogenous in each cell. The traffic information in every time step was first recorded to calculate the average traffic parameters in 30-second period. Then the 30-second traffic parameters were used to calculate the 5-minute traffic variables that were contained in the crash prediction models. In that way the crash risks and the injury severity can be calculated in the CTM-based simulation.

4 OPTIMAL VSL CONTROL STRATEGY

4.1 Development of VSL control strategy

The control logic of the proposed VSL strategy is illustrated in Figure 2. The strategy contains four critical control factors: (1) the control cycle of VSL; (2) the speed reduction factor; (3) the speed change step; and (4) the speed difference between adjacent VSL signs. If the current time reaches the VSL control cycle, the speed limits are calculated and updated on VSL signs. The speed limit in each VSL is calculated according to the speed reduction factor. The change of speed limit is calculated by the speed change step. After

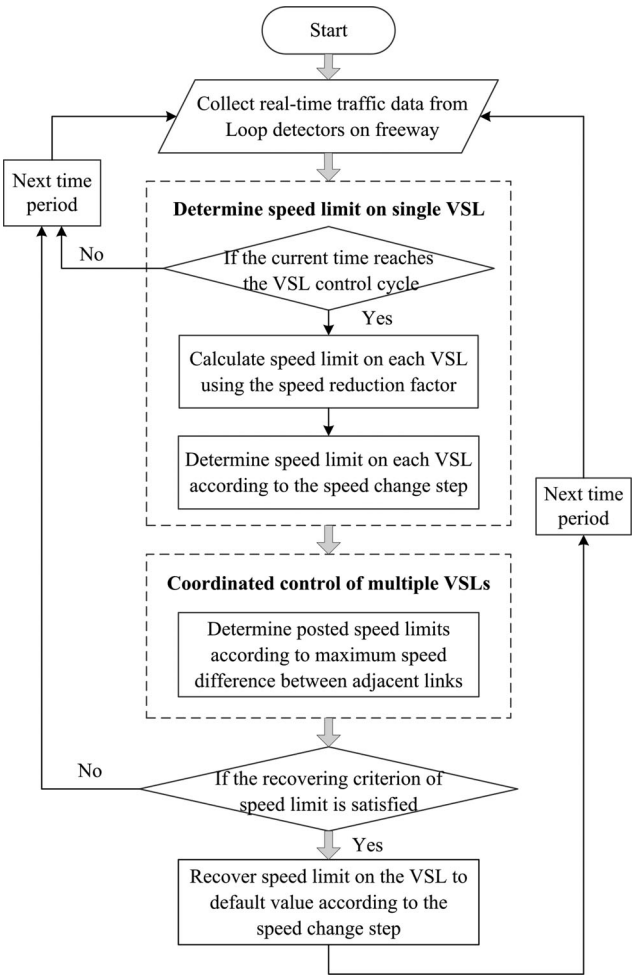

Fig. 2. Control logic of the proposed VSL control strategy.

the speed limit in each single VSL is determined, the coordinated control of multiple VSLs is used to restrict the maximum difference of speed limits between any pair of adjacent VSL signs. The speed limit recovers to the default value if the recovering citation is satisfied. Then the VSL control moves into the next control period and repeats the procedure.

The control cycle determines when the speed limits are updated. A short control cycle means that the speed limits are updated frequently, and vice versa. If the VSL control cycle is reached, the speed limit in each link is updated by:

$$V_{SL}(x_i, t + \Delta t) = V_{SL}(x_i, t) + \Delta V_{SL}(x_i, t) \quad (17)$$

where $V_{SL}(x_i, t + \Delta t)$ is the speed limit at location x_i at time $t + \Delta t$, $V_{SL}(x_i, t)$ is the speed limit at location x_i at time t, and $\Delta V_{SL}(x_i, t)$ is the change of speed limit at location x_i at time t.

The speed reduction factor determines the target speed limit in a link according to the speeds observed at

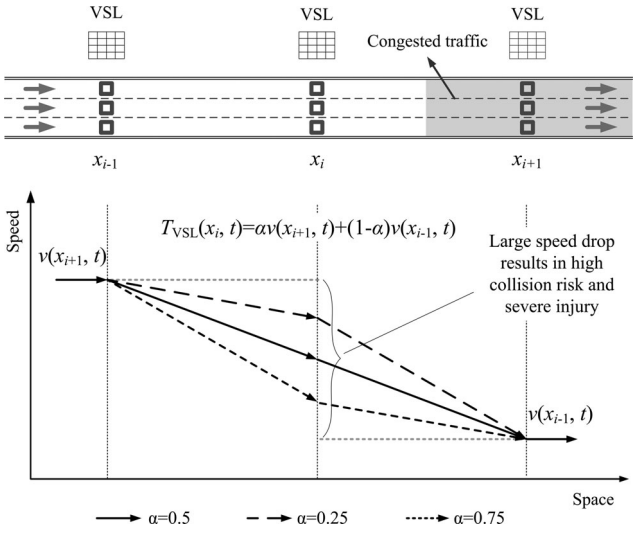

Fig. 3. Scheme for determining target speed limit by speed reduction factor.

its upstream and downstream links. Its purpose is to create a smoothed speed change over space to avoid large and abrupt speed variations. As illustrated in Figure 3, the speed limit at location x_i is determined by adding a fraction parameter to the speeds observed at its upstream location x_{i-1} and its downstream location x_{i+1}, which is:

$$T_{\mathrm{VSL}}(x_i, t) = \alpha v(x_{i+1}, t) + (1 - \alpha)\, v\,(x_{i-1}, t) \quad (18)$$

where $T_{\mathrm{VSL}}(x_i, t)$ is the target speed limit at location x_i at time t, α is the speed reduction factor ($0 < \alpha < 1$), and $v(x_{i+1}, t)$ and $v(x_{i-1}, t)$ are the speeds observed at upstream and downstream detector station locations at time t.

As shown in Figure 3, different factor α leads to different speed reduction results. In general, a larger α means that the speed limit in the link is more close to the observed speed at its downstream link, and vice versa. The speed change step, denoted as ΔV, determines the allowed maximum change of speed limit per control cycle. This factor prevents large change of speed limit which is dangerous to travelers. It also avoids minor but frequent variation of speed limits. The change of speed limit at location x_i at time t is determined by:

$$\Delta V_{\mathrm{SL}}(x_i, t) = -\Delta V, \text{if } T_{\mathrm{VSL}}(x_i, t + \Delta t) < V_{\mathrm{SL}}(x_i, t) - \Delta V \quad (19)$$

$$\Delta V_{\mathrm{SL}}(x_i, t) = \Delta V, \text{if } T_{\mathrm{VSL}}(x_i, t + \Delta t) > V_{\mathrm{SL}}(x_i, t) + \Delta V \quad (20)$$

$$\Delta V_{\mathrm{SL}}(x_i, t) = 0, \text{if } V_{\mathrm{SL}}(x_i, t) - \Delta V < T_{\mathrm{VSL}}(x_i, t + \Delta t) < V_{\mathrm{SL}}(x_i, t) + \Delta V \quad (21)$$

After the change of speed limit in each single VSL is determined according to Equations (17) to (21), the speed difference between adjacent VSL signs, denoted as $\Delta V'$, is examined from the downstream to the upstream links. The change of speed limit at each location x_i at time t is determined by:

$$\Delta V_{\mathrm{SL}}(x_i, t) = -\Delta V', \text{if } T_{\mathrm{VSL}}(x_i, t + \Delta t) > T_{\mathrm{VSL}}(x_{i+1}, t + \Delta t) + \Delta V' \quad (22)$$

The reduced speed limit should be able to recover to the default value when there would be no congestion if the VSL control was not used. The following criterion is used to determine when the speed limit recovers:

$$V_{\mathrm{SL}}(x_i, t) = V_{\mathrm{SL}}(x_i, t) + \Delta V, \text{if } v(x_i, t) < v(x_{i+1}, t) \text{ and } v(x_i, t) = V_{\mathrm{SL}}(x_i, t) \quad (23)$$

Because only discrete values of speed limits are allowed to be posted on VSL signs, the speed limits determined in Equations (22) to (23) are rounded into the nearest 5 mph. Whenever the speed limit exceeds one of its bounds $V_{\mathrm{SL}} \in [V_{\min}, V_{\mathrm{F}}]$, the speed limit is truncated to the respective bound and is used for the next control cycle.

4.2 Procedure for optimizing VSL control factors

The GA is adopted in this study for optimizing the critical control factors of VSL. GA is a search heuristic used to generate useful solutions to optimization and search problems (Goldberg, 1989; Sarma and Adeli, 2001; Putha et al., 2012; Fuggini, et al., 2013; Lin and Ku, 2014; Zhu et al., 2014). The computational procedure that incorporates the GA and the CTM is shown in Figure 4. The procedure starts from testing the randomly selected control factors of VSL in the CTM for the initial population. Then the outputs of the simulation results are evaluated in the GA. The fitness value of every control strategy in the population is evaluated—the fitness is usually the value of the objective function in the optimization problem being solved. The optimal control strategy is identified for the current iteration. If the stopping criteria are met, the optimal control factors are outputted and the procedure ends. If the stopping criteria are not met, the procedure moves to generate new population of control strategies by selecting parents to generate children, children crossover and mutation. The procedure then moves into the next iteration and the new population of control strategies are evaluated.

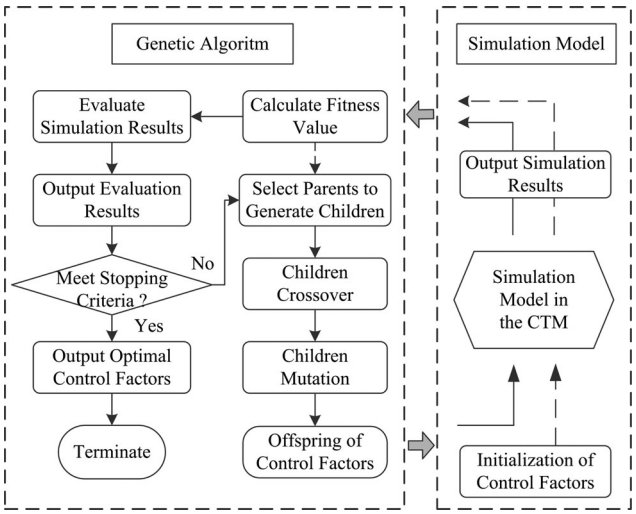

Fig. 4. Algorithm for determining optimal control strategy.

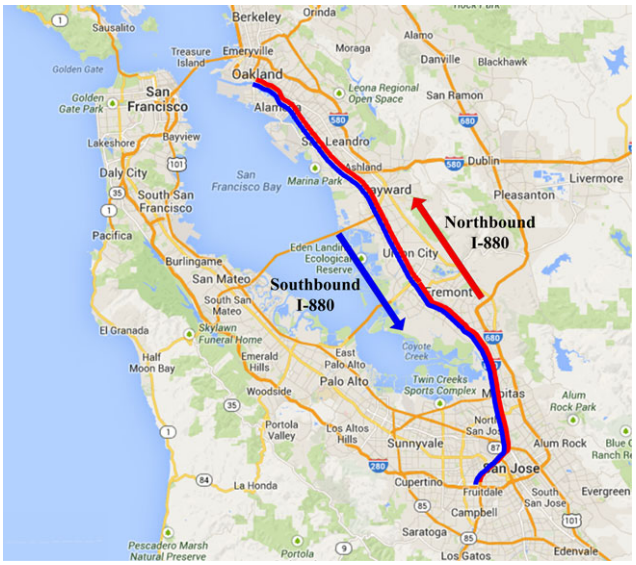

Fig. 5. Study site on Interstate 880 in California.

In this study, the VSL strategy that effectively reduces collision risks and injury severity without significantly increasing travel time is considered the optimum. The fitness function used in the GA is determined by:

$$Fitness = -(\gamma \Delta P + \mu \Delta I + \eta \Delta T) \tag{24}$$

$$\Delta P = [P_{\mathrm{VSL}} - P_{\mathrm{NO}}]/P_{\mathrm{NO}} \tag{25}$$

$$\Delta I = [I_{\mathrm{VSL}} - I_{\mathrm{NO}}]/I_{\mathrm{NO}} \tag{26}$$

$$\Delta TTT = [T_{\mathrm{VSL}} - T_{\mathrm{NO}}]/T_{\mathrm{NO}} \tag{27}$$

$$P = \sum_{t=1}^{T} \sum_{i}^{N} P_{i,t}(crash = 1)/N \times T \tag{28}$$

$$I = \sum_{t=1}^{T} \sum_{i}^{N} I_{i,t}(FI = 1)/M \tag{29}$$

$$I_{i,t}(FI = 1) = \begin{cases} P_{i,t}(FI = 1), & if \quad P_{i,t}(crash = 1) \geq threshold \\ 0, & otherwise \end{cases} \tag{30}$$

$$M = \begin{cases} M + 1, & if \quad P_{i,t}(crash = 1) \geq threshold \\ M, & otherwise \end{cases} \tag{31}$$

where *Fitness* is the fitness value for a VSL strategy, ΔP is the percentage of change in crash risk, ΔI is the percentage of change in injury severity given a crash occurs, ΔTTT is the percentage of change in total travel time, γ, μ, η ($\gamma+\mu+\eta = 1$) are the weight coefficients, P_{VSL}, I_{VSL}, and T_{VSL} are the crash risk, injury severity, and travel time under the VSL control, P_{NO}, I_{NO}, and T_{NO} are the crash risk, injury severity, and travel time in the no control case, $P_{i,t}(\mathrm{crash} = 1)$ is the probability of collision at time t in link i which is calculated by Equations (1) and (3), $I_{i,t}(FI = 1)$ is the probability of FI injury which is calculated by Equations (1) and (4), T is total simulation time period, N is number of links, and *threshold* is used to predict the occurrence of traffic collision.

Injury severity makes sense only when a crash occurs. In this study the injury severity is calculated only when the estimated crash probability exceeds a specified threshold. The threshold is usually determined by considering the trade-off between the prediction accuracy and the false alarm rate (Xu et al., 2013). In our crash risk prediction model, the crash probability of 0.2 achieves a prediction accuracy to be more than 60% and a false alarm rate to be less than 20%. Thus, the crash probability of 0.2 is considered as the threshold in Equations (30) and (31).

5 EXPERIMENT DESIGN

5.1 Freeway network

The study site considered in this study is a 29-mile bi-directional freeway corridor on Interstate 880 in the state of California, United States. The freeway connects two large cities in the Bay Area, which are Oakland and San Jose (see Figure 5). The freeway network contains 59 interchanges in its two directions and 119 inductive loop detector stations with an average spacing of 0.5 mile. The traffic data were obtained from the Freeway Performance Measurement System (PeMS) database

which reported the estimated average speed, flow, and occupancy during 30-second period. Note that the crash prediction models in Section 2 were developed using data from the same freeway sections.

Traffic demands on the freeway of interest are quite large, resulting in considerable travel delays and a large amount of crashes. The speed contour plots in Figure 6 illustrate the typical weekday traffic conditions observed in the two freeway directions. Time and space are shown on the x- and y-axes, respectively, and the color scale represents the estimated time-mean speeds during the day according the legend in the figure. Both freeway directions contain two bottlenecks which typically activate during peak periods. The resulting queues from the bottlenecks increase in length and propagate toward upstream segments. As shown in Figure 6, there are large speed variations on the two freeway sections.

The selected freeway sections were built in the CTM. The total number of mainline cells in the CTM was 580 and the number of cell connectors was 128. The traffic state within every cell was updated per 5.54 seconds in the CTM to predict the traffic dynamic. The peak period in simulation lasts 4 to 5 hours within the two freeway sections. Thus, the examples of the VSL control problem in this study are very complex which require quite large computational effects.

5.2 Placements of VSL signs

The placement of VSL signs may affect the safety effects of VSL. Until recently, little documentation is available regarding how to place the VSL signs on freeway mainlines. In previous studies, the VSL signs were usually placed next to loop detector stations (Lee et al., 2006; Abdel-Aty et al., 2006; Allaby et al., 2007; Hellinga and Mandelzys, 2011; Li et al., 2014b). The freeway sections were then coded as a series of links that corresponded to each detector–VSL pair. The loop detectors gather information about the traffic condition within the link. The VSL sign displays the speed limit for the link. The average spacing of VSL signs in previous studies is usually set to be 0.3 to 0.5 mile.

In this study, three scenarios with different placements of VSL signs were considered to evaluate the safety effects of VSL. The placements of VSL signs on the northbound freeway section are illustrated in Figure 7. In scenario 1, 56 VSL signs are placed on the freeway mainline. The average spacing between adjacent VSL signs is 0.52 mile. In scenario 2, 23 VSL signs are placed within the section with an average spacing of 1.25 miles. Scenario 3 contains only 14 VSL signs with an average spacing of 1.97 miles. Three similar scenarios were also considered for the southbound freeway section. The descriptions of the placements of VSL signs are summarized in Table 1.

6 CALIBRATION OF PARAMETERS

To realistically reproduce the traffic flow characteristics, the parameters in the CTM were calibrated using field data collected from loop detectors on the freeway sections of interest. To calibrate the fundamental diagram in the CTM, four traffic flow parameters need to be identified, which are the free flow speed, the capacity flow, the magnitude of capacity drop at bottleneck, as well as the speed of kinematic wave. The calibrated traffic flow parameters are shown in Table 2. The free flow speed is 65 mph on the selected freeways. The mainline capacity flow is 1,950 veh/h/ln. The magnitude of capacity drop is 6.8%. The speed of kinematic wave is calculated to be 9.2 mph by monitoring the changes of traffic states at loop detector stations (Chung et al., 2007; Zheng et al., 2010).

Two parameters need to be determined to calibrate the stop-and-go traffic in the CTM, which are φ in Equation (13), and ϕ in Equation (14). The objective of calibration is to generate the same magnitude of speed variation in the stop-and-go traffic, which is

$$\min\ Z = \sum_{k=1}^{T}\sum_{i}^{N}\left[\sigma_i^M(k) - \sigma_i^S(k)\right]^2 / N \times T \quad (32)$$

where $\sigma_i^M(k)$ is the measured standard deviation of speed in link i at time k, and $\sigma_i^S(k)$ is the simulated standard deviation of speed in link i at time k. A trial-and-error method was used to determine the two parameters within the range $\varphi \in [0, 1]$ and $\phi \in [0, 1]$. The analysis showed that the speed variation in the stop-and-go traffic in the simulation was reasonably close to the field measurement when the parameter φ was set to be 0.25 and ϕ was set to be 0.1.

As suggested in many previous studies (Lee et al., 2006; Abdel-Aty et al., 2006; Allaby et al., 2007; Li et al., 2014b), the VSL control should consider both the improvement in safety and the decrease in efficiency. In our study this can be done by adjusting the three weight coefficients in Equation (24)—larger weight coefficient means that more importance is paid to that aspect, and vice versa. In our simulation analysis, the weight coefficient $\gamma = 1/3$, $\mu = 1/3$, $\eta = 1/3$ are used to calculate the fitness value for a VSL strategy, assuming that equal importance is paid to the reduction in collision risk, the decrease in injury severity, and the increase in travel time. Local freeway agencies can specify different weight coefficients according to their control objectives between safety and efficiency.

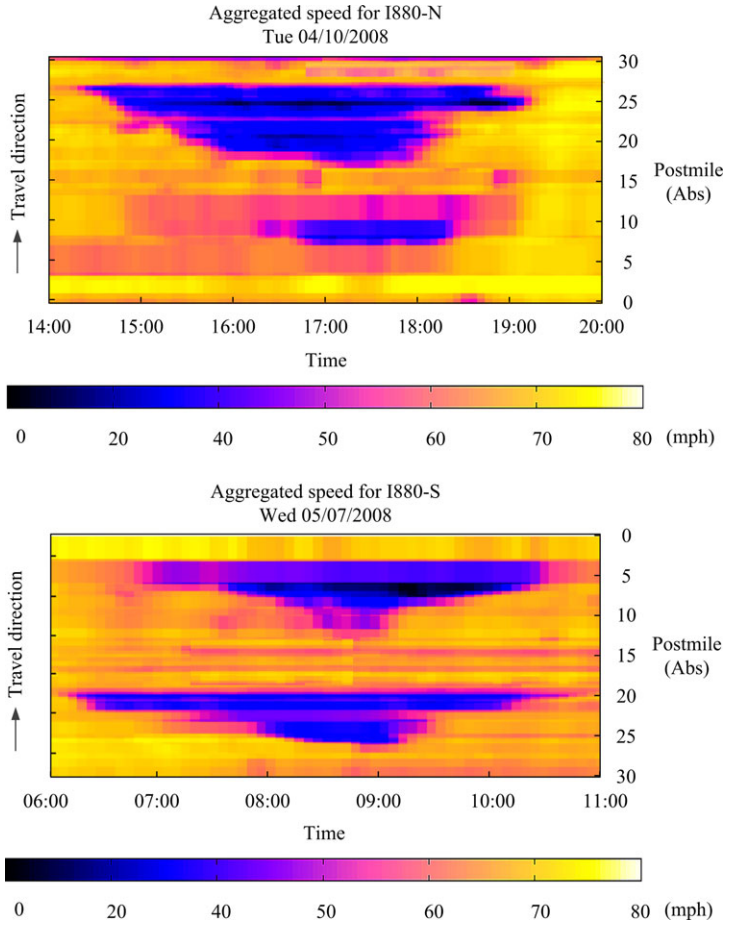

Fig. 6. Speed contour of traffic conditions in two freeway sections.

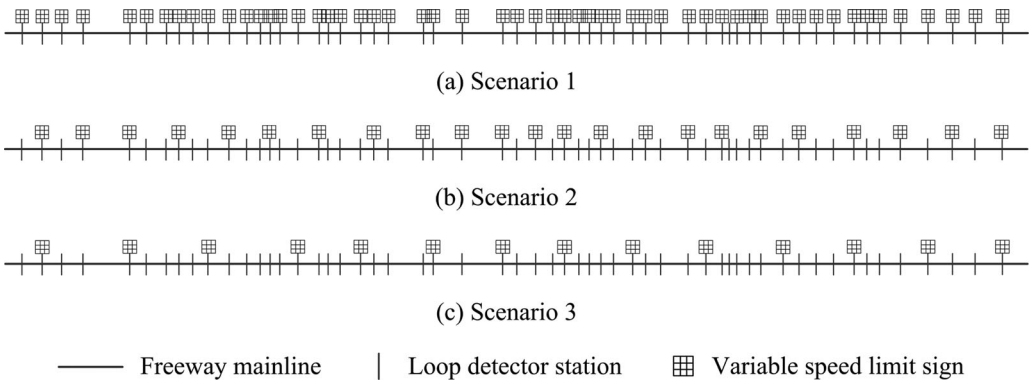

Fig. 7. Deployment of VSL signs in different scenarios on northbound freeway.

Four parameters need to be determined in the GA, including the population number, the maximum generation, the crossover probability, and the mutation probability. In general, larger population and generation could increase the validity of the optimal solution, but could also significantly increase the computing time. In this study, we conducted preliminary analyses to determine the appropriate parameters in the GA. The preliminary analyses suggested that the optimal solution could be obtained in the evolution when the population was set to be 30, the generation was set to be 50, the crossover probability was 0.8, and the mutation probability was 0.1. The evolution process for optimizing VSL control factors is shown in Figure 8.

Table 1
Description of deployment of VSL signs

	Northbound section			*Southbound section*		
Spacing of VSL signs (mile)	*Scenario 1*	*Scenario 2*	*Scenario 3*	*Scenario 1*	*Scenario 2*	*Scenario 3*
Number of signs	56	23	14	56	25	16
Average spacing	0.52	1.25	1.97	0.45	1.17	1.79
Standard deviation of spacing	0.25	0.21	0.38	0.27	0.19	0.31
Minimum spacing	0.20	0.80	1.10	0.20	0.80	1.20
Maximum spacing	1.40	1.70	2.30	1.40	1.70	2.40

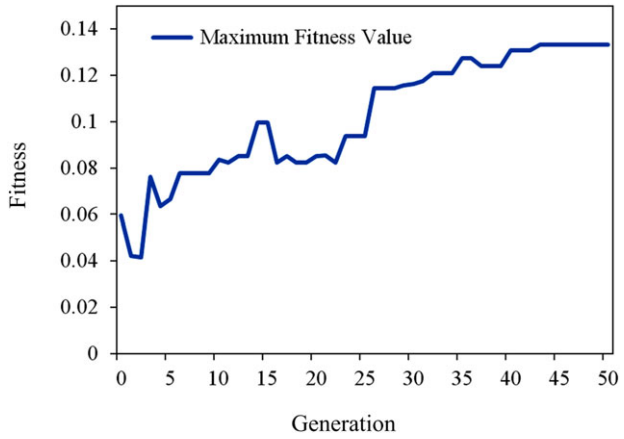

Fig. 8. Fitness value in different generations in the GA.

The fitness value increases gradually as the generation evolves and the optimization process converges in the last several generations. Thus those parameters were considered in the GA for the subsequent analysis in the following sections. Note that the parameters in the GA need to be determined for different scenarios. The same procedure proposed in this study can be followed to optimize the control factors. The running time of the integrated GA and CTM optimization procedure in the preliminary analysis was about 1.5 hours.

7 RESULTS OF SIMULATION ANALYSES

Traffic demands from real data were specified in the CTM to generate the traffic conditions in the two freeway sections. To be consistent with Figure 6, a 6-hour simulation for the northbound freeway section and a 5-hour simulation for the southbound with a 30-minute warm-up period were conducted. Various scenarios with different placements of VSL signs and different drivers' compliances were evaluated. The optimal VSL control strategies were first determined for the northbound freeway section. Then the effects of VSL control were validated for the southbound section.

Table 2
Determination of key parameters

Parameter	*Value or range*
Parameters in CTM	
Free-flow speed	65 mph
Capacity flow	1950 veh/h/ln
Magnitude of capacity drop	6.8%
Speed of kinematic wave	9.2 mph
Parameter φ	0.25
Probability threshold ϕ	0.1
Parameters in GA	
Population number	30
Maximum generation	50
Crossover probability	0.8
Mutation probability	0.1
Control factors in VSL	
Speed reduction factor	0.1 to 0.9
Control cycle of VSL	30 seconds to 5 minutes
Speed change step	5 to 30 mph
Speed difference between adjacent VSL signs	5 to 30 mph

Note: The candidate control factors of VSL are given in Table 2. The speed reduction factor ranges from 0.1 to 0.9 with an increment of 0.05. Five control cycles of VSL are tested including 30 seconds, 1 minute, 2 minutes, 3 minutes, and 5 minutes. Six speed change steps from 5 to 30 mph with an increment of 5 mph are tested. Six speed differences between adjacent VSL signs from 5 to 30 mph are tested.

7.1 Determination of optimal VSL control strategies

Three scenarios with different placements of VSL signs were evaluated. The determined optimal VSL control factors are shown in Table 3. The optimal speed reduction factor in scenario 1 is determined to be 0.85, indicating the posted speed limit is more close to the observed speed at its downstream location. The optimal speed reduction factor in scenarios 2 and 3 is 0.9, which is slightly higher but quite close to that in

Table 3
Optimal control factors determined for northbound section

	Scenarios		
Optimal control factor	*S1*	*S2*	*S3*
Speed reduction factor	0.85	0.9	0.9
Control cycle (second)	30	60	30
Speed change step (mph)	5	10	10
Speed difference between VSLs (mph)	5	5	10

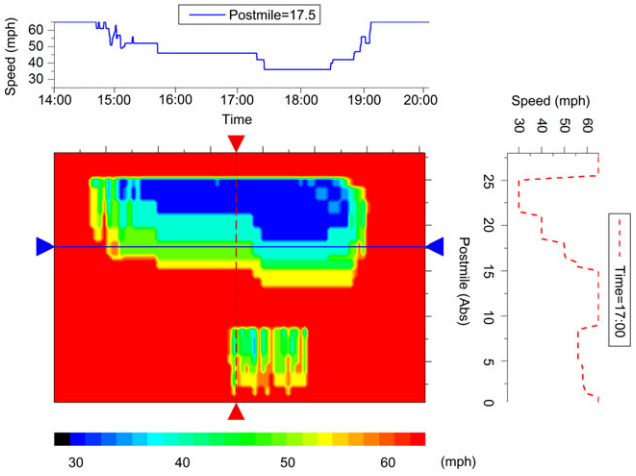

Fig. 9. Contour of speed limit in scenario 2 for the northbound freeway.

scenario 1. The optimal control cycle is 30 to 60 seconds for the three scenarios, suggesting the speed limits should be updated every 30 to 60 seconds. The optimal speed change step is 5 mph in scenario 1, and 10 mph in scenarios 2 and 3. The speed difference between adjacent VSL signs should be 5 to 10 mph to achieve a gradual change of speed limits over space.

The speed limits under the optimal VSL control in scenario 2 are illustrated in Figure 9 as an example to show the VSL control effects. The color scale represents the speed limits according to the legend in the figure. It is observed that the VSL control results in a smoothed change of speed limit over the facility to reduce the large speed reductions on freeways, which is displayed by the gradual change of color. The speed curves in the figure represent the spatial and the temporal changes of speed limits in the optimal VSL control. Figure 9 also shows that the VSL control does not bring in large disturbances to the freeway traffic.

The effects of the optimal VSL control strategies are shown in Table 4. In scenario 1, the VSL control reduces the collision risks by 25.88% and 18.19% for the northbound and southbound sections, respectively,

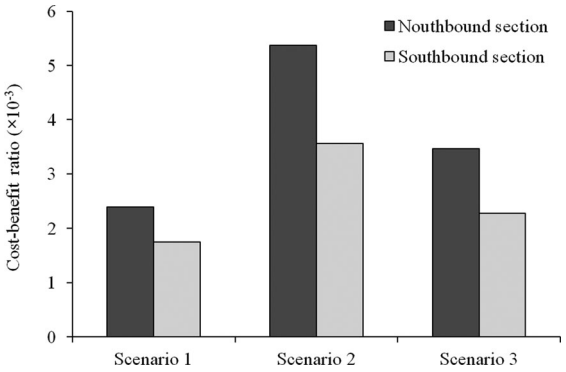

Fig. 10. Results of benefit–cost analysis for different scenarios.

and reduces the injury severity of crashes by 14.71% and 11.62%. The travel time is slightly increased by 0.32% and 0.46% as compared to the condition in which the VSL control is not used. In scenario 2, the VSL control has slightly lower safety effects. The collision risks are reduced by 22.62% and 15.30%, and the injury severity is reduced by 14.67% and 11.76%. In scenario 3, the VSL control has the least safety effects as shown in Table 4. Note that the safety effects of VSL control in the southbound section are lower than those in the northbound section. This is reasonable considering the fact that the optimal VSL control factors are determined for the northbound section.

7.2 Comparison between different placements of VSL signs

The control effects of VSL are affected by the placement of VSL signs. The results in Table 4 suggest that the scenario with more VSL signs is associated with larger safety improvements. The VSL control in scenario 1 results in the largest reduction in the collision risks and the injury severity in either freeway direction. The VSL control successfully reduces the collision risks in scenarios 2 and 3, but does not reduce the injury severity in scenario 3.

The benefit–cost analysis was conducted to compare the control effects of VSL between different scenarios. The benefit–cost ratio used for comparison in this study is defined as the fitness value of the optimal VSL strategy divided by the number of VSL signs. The results of the benefit–cost analysis are shown in Figure 10. The placement of VSL signs in scenario 2 has the highest benefit–cost ratio in either freeway direction, followed by scenario 3 and scenario 1.

The results suggest that it is unnecessary to put excessive VSL signs on freeway mainlines because the

Table 4
Effects of optimal VSL control strategies

	Northbound section			*Southbound section*		
Control effects	*Scenario 1*	*Scenario 2*	*Scenario 3*	*Scenario 1*	*Scenario 2*	*Scenario 3*
Δ% of collision risk	−25.88	−22.62	−10.87	−18.19	−15.3	−7.46
Δ% of injury severity	−14.71	−14.67	−4.06	−11.62	−11.76	−3.76
Δ% of travel time	0.32	0.23	0.36	0.46	0.38	0.28

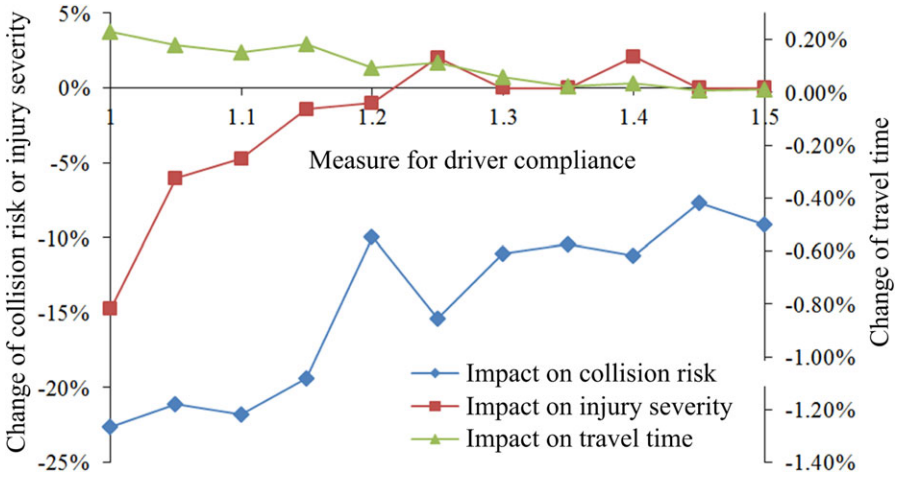

Fig. 11. Control effects of VSL with different driver compliances.

safety benefit is not proportional to the cost. Scenario 1 has a larger number of VSL signs with a smaller average spacing than scenario 2. However, the collision risk in scenario 1 is only reduced by 3.26% and 2.89% as compared to that in scenario 2. The reduction in the injury severity does not change obviously. According to the results of benefit–cost analysis, the VSL placement in scenario 2 is recommended for field application on the selected freeways.

7.3 Effect of drivers' compliances to VSL

The optimal control effects of VSL in the above section were obtained assuming complete drivers' compliances to speed limits posted on VSL signs. However, this assumption is often violated in actual situations. In this section, we evaluated how the effectiveness of the proposed VSL control strategy was affected by the drivers' compliance.

In previous studies, the drivers' compliance to VSL was usually considered by specifying the distribution of individual vehicle speeds in microscopic simulation models (Park and Yadlapati, 2003; Hellinga and Mandelzys, 2011). This study used the CTM to predict the macroscopic traffic flow characteristics. Thus, a different measure was considered to reflect the compliance of drivers. In this study, the measure for drivers' compliance was defined as the ratio of the actual speed divided by the posted speed limit. For example, a measure 1.1 means that if 50 mph is posted on a VSL, the actual average speeds will be 55 mph. By replacing the speed limit $V_{SL}(k)$ in Equations (5) and (9) with the actual speed $V_{SL}'(k)$, the impact of drivers' compliance on traffic flow was reflected in the CTM.

Ten measures for driver's compliance, ranging from 1.1 to 1.5, were evaluated using the optimal VSL control strategy in scenario 2 for the northbound freeway. The curves in Figure 11 show the control effects of VSL. It is found that in general, the safety effects of VSL decrease as the measure for driver compliance increases. The VSL control reduces the collision risks and the injury severity when the measure is smaller than 1.2. The VSL control slightly reduces the collision risks but does not reduce the injury severity when the measure is larger than 1.2.

The results in this section suggest that the drivers' compliance to speed limits significantly affects the safety effects of the optimal VSL control strategy proposed in this study. In practical engineering applications, if drivers on local freeways do not obey VSL, speed

enforcement techniques are recommended used together with the proposed VSL control strategy to achieve the optimum effects on improving freeway safety.

8 CONCLUSIONS AND DISCUSSION

This study developed a computational procedure to determine the optimal VSL control strategies to reduce both the collision risks and the injury severity of crashes on large-scale freeways. The results showed that the proposed VSL control strategies effectively improved traffic safety on freeway mainlines. The optimal VSL control reduced the collision risks by up to 25.88% and reduced the injury severity of crashes by up to 14.71%. The VSL control did not increase the total travel time on freeways. The placements of VSL signs on freeway mainlines significantly affected the control effects of VSL. The safety effects decreased as drivers' compliance rate to the VSL control decreased. The finding suggests the use of speed enforcement techniques together with the VSL control to achieve the optimum control effects.

The optimal VSL strategies proposed in this study were compared to those developed by previous studies. Previous VSL strategies generally recommended using 35 to 45 mph as the target speed limits on VSL (Lee et al., 2006; Abdel-Aty et al., 2006; Allaby et al., 2007; Park and Yadlapati, 2003). In this study, the target speed limit is not a fixed value. The target speed limit is determined dynamically according to the observed speeds at the upstream and downstream links. Thus, the proposed VSL control strategy can accommodate for broader traffic situations on freeways. The speed change rate in previous VSL strategies ranged from 5 mph per 10 minutes to 20 mph per 10 seconds (Abdel-Aty et al., 2006; Allaby et al., 2007; Park and Yadlapati, 2003; Carlson et al., 2011; Li et al., 2014b). In this study, the speed limit is allowed to change by 5 to 10 mph per 30 to 60 seconds. The speed change rate is considered to be faster than some previous studies (Abdel-Aty et al., 2006; Park and Yadlapati, 2003; Lee et al., 2006), but is close to some other studies (Allaby et al., 2007; Carlson et al., 2011). The frequent change of speed limit may lead to unsafe driving conditions when the VSL control is used on actual freeways. We should determine how real traffic responds to speed limit changes and modify the speed change rate accordingly to achieve the desired safety benefits of VSL control. The optimal VSL control strategy uses 5 to 10 mph as the speed difference between adjacent VSL signs which is comparable to several previous strategies (Lee et al., 2006; Carlson et al., 2011), though some other strategies recommended abrupt change of speed limit in space (Abdel-Aty et al., 2006).

The optimal control strategies of VSL proposed in this study has the potential to be used in some freeway dynamic traffic management systems to help reduce the collision risks as well as the injury severity of crashes. Note that the crash prediction models greatly affect the optimal control factors in a VSL. It can be expected that the optimal control factors may change if another crash risk prediction model developed for another freeway is used. This study developed a procedure for optimizing the critical VSL control factors. The same procedure can be followed to optimize the VSL strategy given other crash prediction models. Besides, the optimal VSL control strategies in this study were determined using the weight coefficients of 1:1:1 among the collision risk, the injury severity, and the travel time. Local freeway agencies can specify different weight coefficients according to their control objectives.

Note that the CTM is a kinematic wave model with unbounded deceleration (and acceleration). When congestion propagates upstream, instantaneous deceleration is experimented close to its tails, which may not be consistent with real data. However, the unbounded deceleration in the CTM may not affect the safety effect of VSL because the crash prediction models were determined by aggregated traffic data at finite loop detector station locations. Because the simulation time step and the cell length in our study are very short, the numerical deceleration also smooths the effect of the unbounded deceleration in the CTM. Moreover, the CTM does not reflect the difference in occupancy between different lanes, which was found to be a contributing factor in Equation (3). This may not significantly deviate the results considering the fact that the objective of the proposed VSL control is to reduce the speed differences between upstream and downstream links, not to reduce the difference in occupancy between different lanes. The CTM has limited ability in simulating driver's compliance to speed limits. It is unrealistic to assume that everyone breaks the speed limit by the same value. Thus, microscopic models are more suitable for simulating how driver's compliance to speed limits affects the effects of VSL control. Authors recommend that future studies may focus on those issues.

ACKNOWLEDGMENTS

This research was sponsored by the National Natural Science Foundation of China (Grant No. 51322810). The authors would like to thank the Editor and the anonymous reviewers for their constructive comments and valuable suggestions to improve the quality of the article.

REFERENCES

Abdel-Aty, M., Dilmore, J. & Dhindsa, A. (2006), Evaluation of variable speed limits for real-time freeway safety improvement, *Accident Analysis & Prevention*, **38**(2), 335–45.

Abdel-Aty, M., Uddin, U. & Pande, A. (2005), Split models for predicting multivehicle crashes during high-speed and low-speed operating conditions on freeways, *Transportation Research Record*, **1908**, 51–58.

Adeli, H. & Jiang, X. (2009), *Intelligent Infrastructure – Neural Networks, Wavelets, and Chaos Theory for Intelligent Transportation Systems and Smart Structures*, CRC Press, Taylor & Francis, Boca Raton, FL.

Adeli, H. & Karim, A. (2005), *Wavelets in Intelligent Transportation Systems*, John Wiley and Sons, West Sussex, United Kingdom.

Allaby, P., Hellinga, B. & Bullock, M. (2007), Variable speed limits: safety and operational impacts of a candidate control strategy for freeway applications, *IEEE Transactions on Intelligent Transportation Systems*, **8**(4), 671–80.

Boel, R. & Mihaylova, L. (2006), A compositional stochastic model for real time freeway traffic simulation, *Transportation Research Part B: Mathematical*, **40**, 319–34.

Carlson, R. C., Papamichail, I. & Papageogiou, M. (2011), Local feedback-based mainstream traffic flow control on motorways using variable speed limits, *IEEE Transactions on Intelligent Transportation Systems*, **12**(4), 1261–76.

Cassidy, M. J. & Rudjanakanoknad, J. (2005), Increasing the capacity of an isolated merge by metering its on-ramp, *Transportation Research Part B: Mathematical*, **39**(10), 896–913.

Chung, K., Rudjanakanoknad, J. & Cassidy, M. J. (2007), Relation between traffic density and capacity drop at three freeway bottlenecks, *Transportation Research Part B: Mathematical*, **41**(1), 82–95.

Daganzo, C. F. (1994), The cell transmission model - a dynamic representation of highway traffic consistent with the hydrodynamic theory, *Transportation Research Part B: Methodological*, **28**(4), 269–87.

Fuggini, C., Chatzi, E., Zangani, D. & Messervey, T. B. (2013), Combining genetic algorithm with a meso-scale approach for system identification of a smart polymeric textile, *Computer-Aided Civil and Infrastructure Engineering*, **28**(3), 227–45.

Goldberg, D. E. (1989), *Genetic Algorithms in Search, Optimization and Machine Learning*, Addison-Wesley, Reading, MA.

Gomes, G., Horowitz, R. & Kurzhanskiy, A. A. (2008), Behavior of the cell transmission model and effectiveness of ramp metering, *Transportation Research Part C: Emerging Technologies*, **16**(4), 485–513.

Hadiuzzaman, M. D. & Qiu, T. Z. (2013), Cell transmission model based variable speed limit control for freeways, *Canadian Journal of Civil Engineering*, **40**(1), 46–56.

Hellinga, B. & Mandelzys, M. (2011), Impact of driver compliance on the safety and operational impacts of freeway variable speed limit systems, *Journal of Transportation Engineering, ASCE*, **137**(4), 208–68.

Hooshdar, S. & Adeli, H. (2004), Toward intelligent variable message signs in freeway work zones: a neural network model, *Journal of Transportation Engineering, ASCE*, **130**(1), 83–93.

Jiang, X. & Adeli, H. (2009), Object-oriented model for freeway work zone capacity and queue delay estimation, *Computer-Aided Civil and Infrastructure Engineering*, **19**(2), 144–56.

Kim, T. & Zhang, H., Laval & Daganzo and Leclercq et al (2008), A stochastic wave propagation model. *Transportation Research Part B: Mathematical*, **42**(7–8), 619–34.

Laval, J. A. & Daganzo, C. F. (2006), Lane-changing in traffic streams, *Transportation Research Part B: Mathematical*, **40**(3), 251–64.

Leclercq, L., Laval, J. A. & Chiabaut, N. (2011), Capacity drops at merges: an endogenous model, *in 19th International Symposium on Transportation and Traffic Theory*.

Lee, C., Hellinga, B. & Saccomanno, F. (2003), Real-time-crash prediction model for application to crash prevention in freeway traffic, *Transportation Research Record*, **1840**, 67–77.

Lee, C., Hellinga, B. & Saccomanno, F. (2006), Evaluation of variable speed limits to improve traffic safety, *Transportation Research Part C: Emerging Technologies*, **14**(3), 213–28.

Lee, J., Qian, G. & Chung, E. (2013), Using variable speed limits for motorway off-ramp queue protection, *Presented at the 92th Annual Meeting of Transportation Research Board*, Washington, DC.

Li, J., Chen, Q., Wang, H. & Ni, D. (2009), Analysis of LWR model with fundamental diagram subject to uncertainties. *The 88th Transportation Research Board (TRB) Annual Meeting*, Washington DC.

Li, Y., Ziliaskopoulos, A. K. & Waller, S. T. (1999), Linear programming formulations for system optimum dynamic traffic assignment with arrival time based and departure time based demands, *Transportation Research Record*, **1667**, 52–59.

Li, Z., Chung, K. & Cassidy, M. J. (2013), Collisions in freeway traffic: the influence of downstream queues and interim means to address it, *Transportation Research Record*, **2396**, 1–9.

Li, Z., Li, Y., Liu, P., Wang, W. & Xu, C. (2014a), Development of a variable speed limit strategy to reduce secondary collision risks during inclement weathers, *Accident Analysis & Prevention*, **72**, 134–45.

Li, Z., Liu, P., Wang, W. & Xu, C. (2014b), Development of a control strategy of variable speed limits to reduce rear-end collision risks near freeway recurrent bottlenecks, *IEEE Transactions on Intelligent Transportation Systems*, **15**(2), 866–77.

Lin, D. Y. & Ku, Y. H. (2014), Using genetic algorithms to optimize stopping patterns for passenger rail transportation, *Computer-Aided Civil and Infrastructure Engineering*, **29**(4), 264–78.

Lin, D. Y., Valsaraj, V. & Waller, S. T. (2011), A Dantzig-Wolfe decomposition-based heuristic for off-line capacity calibration of dynamic traffic assignment, *Computer-Aided Civil and Infrastructure Engineering*, **26**, 1–15.

Muñoz, L., Sun, X., Horowitz, R. & Alvarez, L. (2006), Piecewise-linearized cell transmission model and parameter calibration methodology, *Transportation Research Record*, **1965**, 183–91.

Oh, C., Oh, J. & Ritchie, S. (2005), Real-time hazardous traffic condition warning system: framework and evaluation, *IEEE Transactions on Intelligent Transportation Systems*, **6**(3), 265–72.

Oh, S. & Yeo, H. (2012), Microscopic analysis on the causal factors of capacity drop in highway merging sections,

Presented at the 91th Annual Meeting of Transportation Research Boar, Washington DC.

Park, B. & Yadlapati, S. S. (2003), Development and testing of variable speed limit logics at work zones using simulation, *Presented at the 82th Annual Meeting of Transportation Research Board*, Washington DC.

Putha, R., Quadrifoglio, L. & Zechman, E. (2012), Comparing ant colony optimization and genetic algorithm approaches for solving traffic signal coordination under oversaturation conditions, *Computer-Aided Civil and Infrastructure Engineering*, **27**(1), 14–28.

Robinson, M. (2000), Examples of variable speed limit applications, *Presented at the 79th Annual Meeting of Transportation Research Board*, Washington DC.

Sarma, K.C. & Adeli, H. (2001), Bi-level parallel genetic algorithms for optimization of large steel structures, *Computer-Aided Civil and Infrastructure Engineering*, **16**(5), 295–304.

Sumalee, A., Zhong, R. X., Pan, T. L. & Szeto, W. Y. (2011), Stochastic cell transmission model (SCTM): a stochastic dynamic traffic model for traffic state surveillance and assignment, *Transportation Research Part B: Mathematical*, **45**, 507–33.

Tazul Islam, M., Hadiuzzaman, M., Fang, J., Qiu, T.Z. & EI-Basyouny, K. (2013), Assessing mobility and safety impacts of a variable speed limit control strategy, *Presented at the 92th Annual Meeting of Transportation Research Board*, Washington DC.

Ukkusuri, S. & Waller, S. T. (2008), Linear programming models for the user and system optimal dynamic network design problem: formulations, comparisons and extensions, *Networks and Spatial Economics*, **8**(4), 383–406.

Washington, S., Karlaftis, M. & Mannering F. (2010), *Statistical and Econometric Methods for Transportation Data Analysis*. Chapman & Hall/CRC, Boca Raton, FL.

Xu, C., Liu, P., Wang, W. & Li, Z. (2012b), Evaluation of the impacts of traffic states on crash risks on freeways, *Accident Analysis & Prevention*, **47**(1), 162–71.

Xu, C., Tarko, A. P., Wang, W. & Liu, P. (2013), Predicting crash likelihood and severity on freeways with real-time loop detector data, *Accident Analysis & Prevention*, **57**, 30–39.

Xu, C., Wang, W. & Liu, P. (2012a), A genetic programming model for real-time crash prediction on freeways, *IEEE Transactions on Intelligent Transportation Systems*, **99**, 1–13.

Zheng, Z. D., Ahn, S. & Monsere, C. M. (2010), Impact of traffic oscillations on freeway crash occurrences, *Accident Analysis & Prevention*, **42**(2), 626–36.

Zhu, W., Hu, H. & Huang, Z. (2014), Calibrating rail transit assignment models with genetic algorithm and automated fare collection data, *Computer-Aided Civil and Infrastructure Engineering*, **29**(7), 518–30.

NOTATIONS

The following symbols are used in this article:

$P(Y = 1)$ = probability of an event;
$g(x_i)$ = utility function;
x_k = traffic variable k;
β_k = coefficient of variable k;
$P(crash = 1)$ = probability of crash occurrence;
$P(FI = 1)$ = probability of FI injury;
$s_i(k)$ = sending flow in cell i at time k;
$r_i(k)$ = receiving flow in cell i at time k;
k = simulation time;
V_F = free-flow speed;
$V_{SL}(k)$ = speed limit at time k;
$V_{SL}'(k)$ = actual speed at time k;
V_{min} = minimum allowed speed limit;
$d_i(k)$ = density in cell i at time k;
n_i = number of lanes;
Q_{VSL} = maximum flow under current speed limit;
w_i = speed of kinematic wave;
$d_{i,jam}$ = jam density in cell i;
$q_i(k)$ = flow in cell i at time k;
ΔT = simulation time step;
L_i = length of cell i;
d_{VSL} = density associated with flow Q_{VSL};
$o_i(k)$ = occupancy in cell i at time k;
Q_c = capacity flow;
Q_d = maximum discharge flow after capacity drop;
$e(k)$ = stochastic component at time k;
$\varepsilon(k)$ = generated random noise at time k;
φ = parameter which determines the magnitude of the stop-and-go wave;
$\zeta(k)$ = random number within [0, 1];
ϕ = probability threshold;
V_{TH} = speed threshold to determine congestion;
$V_{SL}(x_i, t+\Delta t)$ = speed limit at location x_i at time $t+\Delta t$;
$\Delta V_{SL}(x_i, t)$ = change of speed limit at x_i and t;
Δt = control cycle of VSL;
$T_{VSL}(x_i, t)$ = target speed limit at location x_i at time t;
a = speed reduction factor ($0<\alpha<1$);
$v(x_i, t)$ = speed observed at detector location i at time t;
ΔV = speed change step;
$\Delta V'$ = desired flow with VSL control (veh/h);
Fitness = fitness value for a VSL strategy;
ΔP = percentage of change in crash risk;
ΔI = percentage of change in injury severity;
ΔTTT = percentage of change in total travel time;
γ, μ, η ($\gamma+\mu+\eta = 1$) = weight coefficients;
P_{VSL} = crash risk with VSL control;
I_{VSL} = injury severity with VSL control;
T_{VSL} = travel time with VSL control;
P_{NO} = crash risk in no control case;
I_{NO} = injury severity in no control case;
T_{NO} = travel time in no control case;
$P_{i,t}(\text{crash} = 1)$ = probability of collision at time t in link i;
$I_{i,t}(\text{FI} = 1)$ = probability of FI injury;
T = total simulation time period;
N = number of links;
threshold = probability threshold to predict collision;
$\sigma_i^M(k)$ = measured standard deviation of speed in link i at time k;
$\sigma_i^S(k)$ = simulated standard deviation of speed in link i at time k.